NASA Technical Memorandum 88872

Composite Interlaminar Fracture Toughness: 3-D Finite Element Modeling for Mixed Mode I, II, and III Fracture

Pappu L.N. Murthy
Cleveland State University
Cleveland, Ohio

and

Christos C. Chamis
Lewis Research Center
Cleveland, Ohio

Prepared for the
8th Symposium on Composite Materials Testing and Design
sponsored by the American Society for Testing and Materials
Charleston, South Carolina, April 28-30, 1986

NASA

COMPOSITE INTERLAMINAR FRACTURE TOUGHNESS: THREE-DIMENSIONAL FINITE ELEMENT MODELING FOR MIXED MODE I, II, AND FRACTURE

Pappu L.N. Murthy*
Cleveland State University
Cleveland, Ohio 44115

and

Christos C. Chamis**
National Aeronautics and Space Administration
Lewis Research Center
Cleveland, Ohio 44135

E-3278

SUMMARY

A computational method/procedure is described which can be used to simulate individual and mixed mode interlaminar fracture progression in fiber composite laminates. Different combinations of Modes I, II, and III fracture are simulated by varying the crack location through the specimen thickness and by selecting appropriate unsymmetric laminate configurations. The contribution of each fracture mode to strain energy release rate is determined by the local crack closure methods while the mixed mode is determined by global variables. The strain energy release rates are plotted versus extending crack length, where slow crack growth, stable crack growth, and rapid crack growth regions are easily identified. Graphical results are presented to illustrate the effectiveness and versatility of the computational simulation for (1) evaluating mixed-mode interlaminar fracture, (2) for identifying respective dominant parameters, and (3) for selecting possible simple test methods.

INTRODUCTION

Interlaminar delamination of angleplied laminates is a fracture mode which needs to be carefully examined and properly accounted for in the design of composite structures. Regions prone to delaminations include free edges, locations of stress concentration, joints, inadvertently damaged areas, and defects arising during the fabrication. One way to properly account for interlaminar delamination in design is to determine interlaminar fracture toughness parameters and then to compare these parameters to their respective critical values and to stress states which are likely to induce interlaminar fracture.

Interlaminar fracture in angleplied laminates is generally induced by individual and/or mixed mode type (Modes I-opening, II-shearing, and III-tearing) fracture. In order to properly assess composite fracture resistance, the fracture toughness parameters for each mode and for mixed modes must be known or determined. These parameters can be determined either experimentally or computationally. The unsymmetric double cantilever, the mixed mode flexure and end-notch flexure specimens can be used to experimentally measure mixed

*NASA Lewis Senior Resident Research Associate, Computational Mechanics.
**Senior Research Engineer, Aerospace Structures/Composites.

mode fracture toughness. Variations of these test methods can be used to individually measure Mode I and Mode II. Mode III, on the other hand, is usually measured as a combination with either Mode I or Mode II since Mode III is generally a very difficult test to perform.

A computational procedure (ref.1) was developed at NASA Lewis Research Center for predicting interlaminar fracture in unidirectional composites. This computational procedure consists of three-dimensional finite element analysis in conjunction with composite micromechanics. It is used to determine fracture toughness parameters by computationally simulating respective tests as follows:

Double Cantilever	Mode I
End-notch-flexure	Mode II
Mixed-mode Flexure	Mixed Mode I and II

Recently this computational procedure has been modified to determine mixed Modes I, II, and III in composite laminates. The objective of this report is to describe this modified procedure and its application to composite interlaminar mixed mode fracture.

The modified procedure consists of three-dimensional finite element analysis in conjunction with integrated composite mechanics (micromechanics, macromechanics, combined-stress failure criteria, and laminate theory). The procedure is used to computationally simulate the mixed-mode fracture of flexural specimens made from unsymmetric/unbalanced laminate configurations. Different combinations of Modes I, II, and III are simulated by varying the crack location through the specimen thickness and by selecting appropriate unsymmetric laminate configurations. The contribution of each fracture mode is determined by local crack closure methods while the mixed mode is determined from the global method. The fracture modes are determined in terms of strain energy release rates. The strain energy release rates are plotted versus extending crack length, where slow crack growth, stable crack growth, and rapid crack growth regions are easily identified. Graphical results are also presented which illustrate the effects of parameters such as: (1) ply orientation, (2) laminate configuration, (3) interlaminar crack location, and (4) laminate material-coupling coefficients on strain energy release rates. Fundamental considerations and possible generalizations are also described.

COMPUTATIONAL SIMULATION: FUNDAMENTAL CONSIDERATIONS

The computational simulation method for evaluating interlaminar individual and mixed mode fracture toughness consists of three-dimensional finite element analysis, including finite element local mesh refinement, and integrated composite mechanics. Several fundamental considerations are associated with this computational simulation method. These fundamental considerations include: (1) laminate configurations, (2) component geometry and loading, (3) finite element model, (4) composite system, and (5) computational procedure. Each of these are described below.

Laminate Configurations

The laminate configurations used in these studies were unbalanced, unsymmetric $[-\theta_m/+\theta_n]$. These laminates were selected in order to evaluate

the effects of the different laminate material-coupling coefficients, in the laminate force deformation relationships, on the individual and mixed mode fracture strain energy release rates (SERR).

The force deformation relationships are given by the following matrix equation (ref. 2):

$$\begin{Bmatrix} \{N\} \\ \hline \{M\} \end{Bmatrix} = \left[\begin{array}{c|c} [A] & [C] \\ \hline [C] & [D] \end{array}\right] \begin{Bmatrix} \{\varepsilon_o\} \\ \hline \{\kappa\} \end{Bmatrix} + \Delta M \begin{Bmatrix} \{N_M\} \\ \hline \{M_M\} \end{Bmatrix} + \Delta T \begin{Bmatrix} \{N_T\} \\ \hline \{M_T\} \end{Bmatrix} \qquad (1)$$

The notation in equation (1) is as follows:

{N} denotes the section (know or calculated from eq. (1)) membrane or axial forces (N_{xx}, N_{yy} and N_{xy}) along the respective structural axes; {M} denotes the corresponding bending moments; [A], [C], and [D] denote membrane, coupled bending-membrane and bending stiffness [3 x 3] matrices, respectively; $\{\varepsilon_o\}$ denotes the mid plane strains (ε_{xxo}, ε_{yyo}, ε_{xyo}); $\{\kappa\}$ denotes the laminate structural axes curvatures (κ_{xx}, κ_{yy}, and κ_{xy}); ΔM and ΔT denote changes in moisture and temperature, respectively; $\{N_M\}$ and $\{M_M\}$ denote axial forces and bending moments due to moisture gradient through-the-laminate-thickness; and $\{N_T\}$ and $\{M_T\}$ denote forces and moments due to corresponding temperature gradient. The material-coupling coefficients which couple the different fracture modes are: (1) A_{13} for N_{xx}/N_{xy} (Mode II/Mode III) coupling, (2) A_{23} for N_{yy}/N_{xy} (Mode II/Mode III) coupling, (3) C_{13} for N_{xx}/M_{xy} (Mode II/Mode I and Mode III) coupling, (4) C_{23} for N_{yy}/M_{xy} (Mode II/Mode I and Mode III) coupling, (5) D_{13} for M_{xx}/M_{xy} (Mode I and Mode II/ Mode II and Mode III) coupling, and (6) D_{23} for M_{yy}/M_{xy} (Mode I and Mode II/ Mode II and Mode III) coupling.

The specific laminates studied are summarized in table 1. Seven cases ($[-\Theta_{36}/+\Theta_{12}]$, Θ = 0°, 15°, 30°, 45°, 60°, 75°, and 90°) were investigated for the laminate configuration effects on the SERR. At the Θ = 45° position, a total of three cases ($[-45_m/45_{12}]$, m = 36, 60 and 84) were investigated for the interlaminar crack location effects on SERR. It is important to note that these specific laminate configurations and the interlaminar crack locations were selected only for computational simulation convenience. They represent just one application of the present procudure.

Component Geometry and Loading

The geometric configuration and the loading of the component selected for the studies are shown in figure 1. This component, dimensions and loading were selected because: (1) it is the same specimen used for measuring interlaminar and mixed mode (I and II) fracture toughness as described in reference 1; (2) it is one of the simplest component-loading condition combinations that can be used to computationally evaluate the effects of laminate configuration, material-coupling and interlaminar crack (delamination) location on individual (Mode II) and mixed mode fracture (Modes I and II and Modes I, II, and III) SERR; and (3) it is readily amenable to conduct experimental studies for composite system screening and the determination of environmental effects.

Finite Element Model

The computational simulation was performed using MSC/NASTRAN with local mesh refinement. A computer plot of the finite element model is shown in figure 2. The entire component with the supports and typical overhang is modeled. The finite element model consisted of 1856 solid elements, 2450 nodes, and 7350 degrees-of-freedom (DOF). This finite element model is similar to that used in reference 1 but with variable thickness elements. A frontal view of the finite element model showing the local details and the location of the mesh refinement "superelement" is shown in figure 3. A schematic of the local superelement is shown in figure 4 where its characteristics are also summarized. It is worth noting that the local model includes solid elements for the interlaminar matrix layer. The inclusion of the interlaminar matrix layer and the anaylsis of the entire specimen are two unique features which distinguish the computational simulation method described herein from what is conventionally done and reported in the literature.

Composite System

The laminates are assumed to be made from a composite material consisting of AS graphite-fibers in an intermediate-modulus high-strength epoxy (AS/E) with a 0.6 fiber volume ratio (FVR). The composite material properties required for the three-dimensional finite element analysis were generated using the (integrated composite analyzer) computer code (ICAN) rising typical (ref. 2) constituent material properties summarized in table 2. These properties are encoded as subsets of the ICAN resident data bank. The three-dimensional MSC/NASTRAN material card properties generated by ICAN are summarized in table 3 using the NASTRAN notation. Note that the last entry in table 3 is the interlaminar (interply) layer thickness which is predicted by ICAN and which is the finite element thickness for this layer. Using integrated composite mechanics to predict the requisite three-dimensional finite element material properties and the interply layer thickness are two additional unique features of the present computational simulation method.

Computational Procedure

The computational procedure used is that developed previously (ref.1) modified to accommodate unsymmetric laminates for Mode III fracture. It consists of a global method for determining mixed mode fracture SERR and the local crack closure method for determining the contributions of the individual modes fracture SERR. Each method is summarized below for completeness.

Global Method

The specific computational steps for this method are as follows (refer to fig. 1):

(1) Model the component with crack length "a" using three-dimensional finite elements.

(2) Apply a load (P) at component midspan.

(3) Calculate the midspan displacement $w(a)$ (w as a function of "a") using three-dimensional finite element analysis (FEA).

(4) Induce crack extension Δa keeping load (P) constant.

(5) Calculate the midspan deflection $[w(a + \Delta a)]$.

(6) Determine the Strain Energy Release Rate (SERR), G_T, from

$$G_T = P \frac{[w(a + \Delta a) - w(a)]}{2b \ \Delta a} \tag{2}$$

where b is the specimen width.

(7) Repeat steps (4) to (6).

(8) Plot results for G_T versus a or Δa.

(9) Identify fracture toughness characteristics as described in reference 1.

(10) Examine complete stress state near crack tip.

(11) Compare with corresponding uniaxial composite strengths.

(12) Look for possible correlation of fracture toughness parameters with composite uniaxial strengths.

The global method yields the global "fracture toughness" SERR without any regard to participating and/or dominating local fracture modes.

Local Closure Method

The specific steps for this method are as follows:

(1) Perform steps (1) and (2) as in the Global Method.

(2) Calculate displacements $(u(a), v(a), w(a)$ at the crack tip nodes using FEA.

(3) Induce crack extension Δa keeping P constant.

(4) Calculate $(u(a + \Delta a), v(a + \Delta a), w(a + \Delta a))$ at the same nodes as in step (2).

(5) Apply enforced displacements (single point constraints) using the step (2) displacements $(u(a), v(a), w(a))$ at the crack tip nodes.

(6) Repeat FEA with these single point constraints.

(7) Calculate the corresponding forces at these constraints (F_x, F_y, F_z). These are called the single point constraint forces in FEA.

(8) Determine the local SERR's from

$$G_I = F_z \frac{[w(a + \Delta a) - w(a)]}{2b \quad \Delta a} \tag{3}$$

$$G_{II} = F_x \frac{[u(a + \Delta a) - u(a)]}{2b \quad \Delta a} \tag{4}$$

$$G_{III} = F_y \frac{[v(a + \Delta a) - v(a)]}{2b \quad \Delta a} \tag{5}$$

(9) Repeat steps (3) to (8).

(10) Follow steps (8) to (12) in the Global Method.

The local crack closure method yields the contribution of each local fracture mode to the composite mixed mode fracture toughness (SERR).

RESULTS AND DISCUSSION

The primary result of this study is the demonstration of the effectiveness and versatility of the computational simulation method. The results presented herein evaluate composite structure and material factors that influence individual and mixed mode interlaminar fracture. These factors include: (1) interlaminar crack opening (a), (2) ply orientation (θ), (3) laminate configuration ($[-\theta/+\theta]$), (4) interlaminar (interply) crack location ($[\theta_m/+\theta_n]$), (5) material-coupling coefficients, and (6) three-dimensional stress state ahead of the crack tip. Each of these factors are described below in terms of their effects on individual and mixed mode fracture SERR relative to component and loading in figure 1.

Effects of Crack Opening

The effects of crack opening on the individual mode fracture SERR (G_I, G_{II} and G_{III}) and mixed mode SERR (G_T) are plotted in figure 5 for the seven different laminate configurations, $[-\theta_{36}/+\theta_{12}]$, ($\theta$ = 0°, 15°, 30°, 45°, 60°, 75° and 90°), figures 5(b) to (f), respectively, assuming a 480 lb load. The important observations in figures 5(b) to (f) are: (1) the shearing fracture Mode II (G_{II}) dominates the stable crack propagation (growth); (2) the opening fracture Mode I (G_I) dominates the rapid crack propagation; (3) the tearing fracture Mode III (G_{III}) has generally similar form as the shearing mode (G_{II}) but of considerably lower magnitude (about 10 percent), and (4) the mixed mode fracture (G_T) is <u>not</u> the algebraic sum of the other three and, therefore, needs to be determined using a global method.

The important conclusions are: (1) a global method should be used to determine the mixed mode fracture, (2) local methods effectively determine the contribution of the individual fracture modes, and (3) local methods can be used to determine the crack opening range in which the different fracture modes dominate. One significant implication from the above observations/conclusions is that local averaging methods, such as: crack opening, J integral, stress intensity, intense energy parameters, and inherent material flaw parameters used to estimate global fracture parameters, will generally underestimate the

mixed mode fracture as defined by SERR G_T. Use of these local averaging methods will result in an optimistic estimate of the composite structure interlaminar fracture toughness. The loss in energy in the removed interply layer elements contributes about three percent to this optimistic estimate. Experimental data obtained by using local measuring techniques should be interpreted with the above implication in mind.

Effects of Ply Orientation

The effects of ply orientation on the maximum individual and mixed mode fracture SERR (assuming a 480 lb load) are plotted in figure 6 for the seven cases of the $[-\theta_{36}/+\theta_{12}]$ (θ = 0°, 15°, 30°, 45°, 60°, 75° and 90°) AS/E laminate. The relative dominance of the opening fracture mode SERR (G_I) and the negligible contribution of the tearing fracture mode SERR (G_{III}) on the maximum mixed fracture mode SERR (G_T) are clearly observed in this figure. Another observation is that the "maximum" magnitude of mixed mode fracture (G_T) levels off at ply angle orientations greater than 60° ($\theta > 60°$).

The above observations lead to the following conclusions: (1) the rapid or unstable interlaminar crack growth is dominated by the opening fracture mode; (2) the tearing fracture mode SERR (G_{III}) is negligible compared to G_T for ply orientation angles greater than 60°; (3) the individual fracture modes (G_I and G_{II}) and the mixed mode fracture are practically independent of ply orientation angle greater than 60°; and (4) ply orientation angles less than 60° have significant influence on the SERR of individual fracture mode and to mixed mode fracture.

Effects of Laminate Configuration

The effects of the laminate configuration on the SERR due to a 480 lb load are shown in figure 7. The effects on the individual fracture mode SERR's are plotted in figures 7(a) to (c). The SERR for the mixed fracture mode (G_T) is plotted in figure 7(d). The important observations in this figure are: (1) the shearing mode fracture SERR (G_{II}) appears to reach a maximum and then decrease with increasing crack opening for practically all the laminate configurations, (2) the tearing mode fracture SERR (G_{III}), on the other hand, continues to increase with crack length for some laminate configurations.

The conclusion from the above discussion is that laminate configurations can be selected for "stable" shearing and tearing fracture mode crack growth for given composite components and loadings. It is important to keep in mind that advantages of this can be taken only in the absence of opening mode fracture.

Effects of Interlaminar Crack Location

Recall that the effects of the interlaminar crack location are studied using the laminate $[-\theta_m/+\theta_{12}]$. For these studies θ is chosen to be 45° since the laminate configuration with this ply angle had the greatest magnitude of tearing mode fracture SERR (G_{III}) (see fig. 7(c)). Results obtained are shown in figure 8 for three different crack locations (m = 36, 60, and 84)

as defined in table 1. The loads corresponding to these crack locations were: 480, 882, and 1358 lb, respectively, in order to subject the laminates to approximately constant external work.

The effects of crack location on the individual mode fracture SERR (G_I, G_{II} and G_{III}) are plotted in figures 8(a) to (c). That for the mixed mode fracture SERR (G_T) is plotted in figure 8(d). Collectively these results show that the effects of the interlaminar crack location on the SERR decrease as the thickness above the crack plane increases. These effects are more pronounced for the opening and tearing modes fracture SERR than they are for the shearing mode fracture.

The above discussion leads to the following important conclusion: laminates subjected to bending can sustain relatively large interlaminar cracks when these cracks are located near the tensile surface of laminate. The significant implication of this conclusion is that relatively large interlaminar crack sizes are detectable by available NDE inspection methods. And, therefore, this computational simulation methods may be used to establish guidelines for setting fracture control requirements, for example, size of allowable delamination versus depth from surface.

Effects of Material-Coupling Coefficients

The tearing mode fracture is present in unbalanced, unsymmetric laminates when subjected to bending loads as was already mentioned. The magnitude of the tearing mode fracture SERR depends strongly on the magnitude of material-coupling coefficients such as A_{23}, and C_{23}. However, these coupling coefficients generally are present in combinations with their complements and with other material-coupling coefficients A_{13}, C_{13}, D_{13} and D_{23}.

The effects of ply orientation in a $[-\theta_{36}/+\theta_{12}]$ laminate on the material-coupling coefficients are shown in figure 9. The effects on axial normal-shear coupling A_{13} and A_{23} are plotted in figure 9(a). The effects on membrane-bending coupling C_{13} and C_{23} are plotted in figure 9(b). The effects on bending-twisting coupling D_{13} and D_{23} are plotted in figure 9(c). As can be seen in figure 9 the 13 and 23 coupling coefficients are complementary, and vanish at $\theta = 30°$ or $90°$.

The effects (variations) of the coupling coefficients on the opening mode fracture SERR (G_I) due to a 480 lb load are shown in figure 10. The effects of A_{13}, C_{13} and D_{13} are plotted in figure 10(a), (b), and (c), respectively. As can be seen in these plots G_I is a double-value function of the material-coupling coefficients. This double-value function results from the complimentary parts of the material-coupling coefficients mentioned previously.

Comparable plots for the effects on the shearing mode fracture SERR (G_{II}) are shown in figure 11. These effects are similar to those for the opening mode. The effects of the material-coupling coefficients on the tearing mode fracture SERR (G_{III}) are shown in figure 12. These effects are also double-value functions and reach their maximum magnitude at $\theta = 45°$.

The important conclusion from the results in figures 11 and 12 is that laminate configurations exist which exhibit considerable tearing mode fracture SERR (G_{III}) in flexural components which are subjected to bending loads. It

is possible, therefore, to determine the magnitude of this mode by simple experimental techniques. This magnitude will not be measured individually. It will be in combination with the other two modes.

Three-Dimensional Stress State

The individual fracture modes are caused by individual, or combination of stresses at the crack tip. The dominant stress for each respective mode can be determined by plotting the three-dimensional stress state versus distance from the crack tip. The three-dimensional stress state is computed as a part of the three-dimensional finite element analysis. This procedure is illustrated in figure 13 where the three-dimensional stress state in the interply layer ahead of the crack tip is shown for the $[-30_{36}/+30_{12}]$ laminate.

The important observations in figure 13 are: (1) σ_{zx} has the highest magnitude (about -25 ksi); (2) σ_{zz} has the second highest magnitude (about 14 ksi); the magnitudes of the other stresses in decreasing order are as follows: σ_{xx} approximately 8 ksi, σ_{yy} approximately 5 ksi, σ_{yz} approximately 4 ksi and σ_{xy} approximately 0. The dominant stresses, therefore, which cause interlaminar fracture growth and their corresponding fracture modes are as follows (dominant-stress/fracture-mode):

1. "Longitudinal" interlaminar shear stress/shearing fracture mode (σ_{zx}/G_{II})

2. Interlaminar normal stress/opening fracture mode (σ_{zz}/G_{I})

3. "Transverse" interlaminar shear stress/tearing fracture mode (σ_{yz}/G_{III})

The in-plane stresses also contribute to the individual fracture modes. Following the above notation their contributions are:

1. σ_{xx}/G_{II} and G_{I}

2. σ_{yy}/G_{III}

3. $\sigma_{xy} = 0$ and, therefore, does not contribute; otherwise it contributes to G_{III}.

The plots in figure 13 can also be used to estimate stress magnitudes at which crack propagation will occur. This is accomplished by plotting the corresponding ply strengths. For example the longituding interlaminar shear strength for this composite is about 13 ksi. The transverse interlaminar shear strength is about 9 ksi. The normal interlaminar stress is about 6 ksi. Comparing the dominant stress magnitudes it is found that:

σ_{zx} approximately 25 ksi > 13 ksi; σ_{zz} approximately 14 ksi > 7 ksi; and σ_{yz} approximately 5 ksi < 9 ksi. Therefore, it may be concluded that crack propagations will occur due to the shearing and opening fracture modes.

SUMMARY

The significant results and conclusions of an investigation to computationally simulate composite interlaminar individual and mixed-mode fracture toughness as determined by strain energy release rates (SERR) are summarized below.

1. The individual and mixed mode fracture SERR can be readily determined using a computational simulation procedure that consists of three-dimensional finite element analysis and integrated composite mechanics.

2. Individual and mixed mode fracture SERR magnitude of $[-\theta_m/+\theta_n]$ are strongly influenced by crack length, ply angle, and interlaminar crack location. However, the maximum magnitude of the mixed mode fracture SERR (G_T) is practically independent for ply orientations greater than 60°.

3. The tearing fracture mode SERR (G_{III}) has the smallest magnitude compared to opening (G_I) and shearing (G_{II}) fracture modes for this case. The tearing fracture mode is generally present in combinations with other fracture modes.

4. The individual and mixed mode fracture SERR decrease as the location of the interlaminar crack approaches the tensile surface of a laminate which is subjected to bending.

5. The magnitudes of the material coupling coefficients strongly influence the individual and mixed mode fracture SERR. The presence of these coefficient magnitudes induce tearing mode fracture in combination with other fracture modes when the component or specimen is subjected to in-plane or bending loads.

6. The dominant stresses associated with individual fracture modes are readily identified from the three-dimensional finite element analysis results.

7. Laminate configurations can be selected which exhibit substantial tearing fracture mode in a three-point-bend specimen, and therefore, the magnitude of this mode can be determined by simple experiments.

8. Stress magnitudes ahead of the crack tip can be compared with corresponding local laminate strengths in order to determine the dominant stress which drives the crack.

9. Local averaging methods/techniques may provide optimistic estimates of global fracture toughness critical parameters.

10. Collectively the results demonstrate that the procedure described herein can be used to computationally simulate/evaluate mixed mode fracture toughness parameters in composite components subjected to complex loadings.

REFERENCES

1. P.L.N. Murthy and C.C. Chamis; "Interlaminar Fracture Toughness: ThreeDimensional Finite-Element Modeling for End-Notch and Mixed-Mode Flexure," NASA TM-87138, National Aeronautics and Space Administration, Washington, D.C., 1985.

2. P.L.N. Murthy and C.C. Chamis; "Integrated Composite Analyzer (ICAN) - Users and Programmers Manual," NASA TP-2515, National Aeronautics and Space Administration, Washington, D.C., 1986.

TABLE I. - LAMINATE CONFIGURATIONS

No.	Configuration	Total thickness, in.	Crack location from bottom surface, in.
1.	$[0_{36}/0_{12}]$	0.24	0.06
2.	$[-15_{36}/+15_{12}]$	↓	↓
3.	$[-30_{36}/+30_{12}]$		
4.	$[-45_{36}/+45_{12}]$		
5.	$[-60_{36}/+60_{12}]$		
6.	$[-75_{36}/+75_{12}]$		
7.	$[-90_{36}/+90_{12}]$	↓	
8.	$[-45_{60}/+45_{12}]$	0.36	
9.	$[-45_{84}/+45_{12}]$	0.48	0.06

TABLE II. - TYPICAL CONSTITUENT MATERIAL PROPERTIES USED IN THE SIMULATION

Property	Units	Fiber AS-graphite		Matrix intermediate-modulus high-strength	
		Symbol	Value	Symbol	Value
Elastic moduli	$\times 10^6$ psi	E_{f11}	31	E_m	0.5
		E_{f22}	2		
		G_{f12}	2		
		G_{f23}	1	G_m	.185
Poisson's ratio	--------	V_{f12}	0.2	V_m	.35
		V_{f23}	0.25		
Strengths	ksi	S_{fT}	400	S_{mT}	15
		S_{fc}	400	S_{mc}	35
Fiber diameter	inch	d_f	0.0003	S_{ms}	13

TABLE III. - MATERIAL PROPERTIES FOR THREE-DIMENSIONAL FINITE ELEMENT ANALYSIS

[ICAN predicted, reference 2.]

Property	Units	Symbol (MSC/NASTRAN)	Laminate configuration						
			0	±15	±30	±45	±60	±75	±90
Elastic	mpsi	G_{11}	19.080	16.840	11.500	6.035	2.692	1.589	1.469
constants in		$G_{21} = G_{12}$	0.546	1.607	3.728	4.788	3.728	1.607	0.546
the stress/		$G_{31} = G_{13}$	0.546	0.552	0.567	0.589	0.610	0.626	0.631
strain		$G_{41} = G_{14}$	0.000	±4.039	±5.650	±4.404	±1.968	±0.365	0.000
relationship		$G_{51} = G_{15}$	0.000	0.000	0.000	0.000	0.000	0.000	0.000
for AS/E		$G_{61} = G_{16}$	0.000	0.000	0.000	0.000	0.000	0.000	0.000
composite		G_{22}	1.469	1.589	2.692	6.035	11.500	16.840	19.080
(FVR 0.6)		$G_{32} = G_{23}$	0.631	0.626	0.610	0.589	0.567	0.552	0.546
		$G_{42} = G_{24}$	0.000	±0.365	±1.977	±4.404	±5.650	±4.039	0.000
		$G_{52} = G_{25}$	0.000	0.000	0.000	0.000	0.000	0.000	0.000
		$G_{62} = G_{26}$	0.000	0.000	0.000	0.000	0.000	0.000	0.000
		G_{33}	1.469	1.469	1.469	1.469	1.469	1.469	1.469
		$G_{43} = G_{34}$	0.000	∓0.021	∓0.037	∓0.043	∓0.037	∓0.022	0.000
		$G_{53} = G_{35}$	0.000	0.000	0.000	0.000	0.000	0.000	0.000
		$G_{63} = G_{36}$	0.000	0.000	0.000	0.000	0.000	0.000	0.000
		G_{44}	0.623	1.684	3.805	4.865	3.805	1.684	0.623
		$G_{54} = G_{45}$	0.000	0.000	0.000	0.000	0.000	0.000	0.000
		$G_{64} = G_{46}$	0.000	0.000	0.000	0.000	0.000	0.000	0.000
		G_{55}	0.362	0.380	0.428	0.493	0.558	0.606	0.623
		$G_{65} = G_{56}$	0.000	∓0.065	∓0.113	∓0.131	∓0.113	∓0.065	0.000
		G_{66}	0.623	0.606	0.558	0.493	0.428	0.380	0.362
Interply	mpsi	E	0.5	------	------	------	------	------	------
Layer	----	ν	0.35	------	------	------	------	------	------

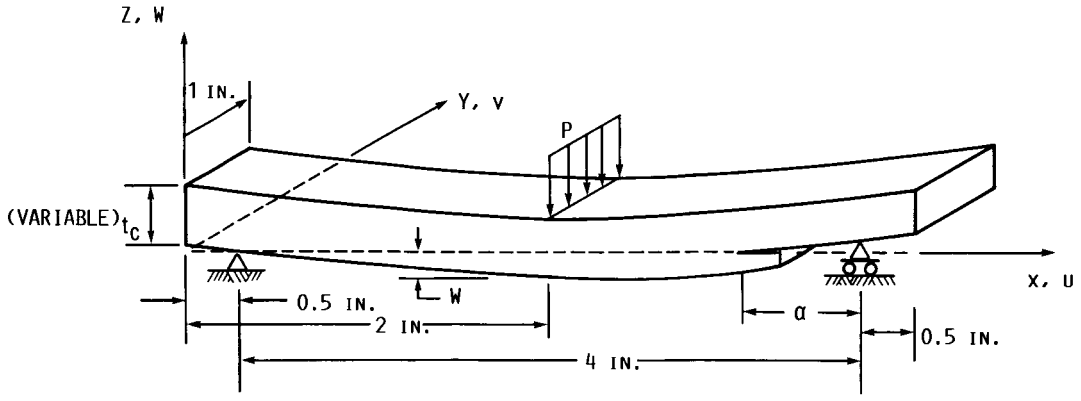

FIGURE 1.- COMPONENT GEOMETRY AND LOADING SCHEMATIC.

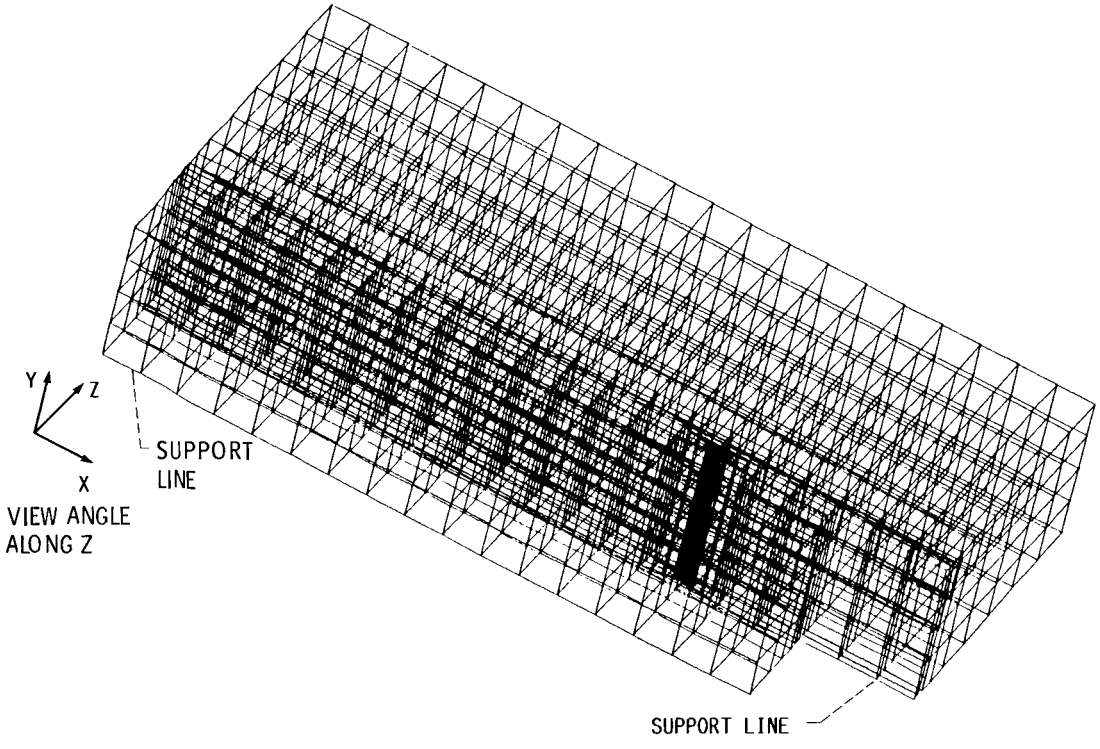

FIGURE 2.- COMPUTER PLOT OF COMPONENT 3-D FINITE ELEMENT MODEL (1856 SOLID ELEMENTS: 32-PENTAHEDRONS, 1824 HEXAHEDRONS, 2450 NODES,7350 DEGREES-OF-FREEDOM (DOF)).

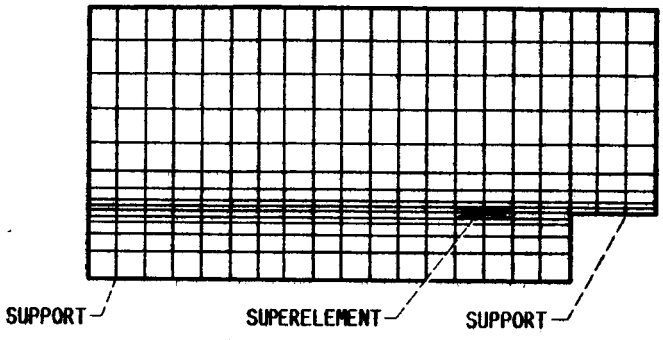

FIGURE 3.- FRONTAL VIEW OF FINITE ELEMENT MODEL SHOWING LOCATION AND GRID OF SUPERELEMENT.

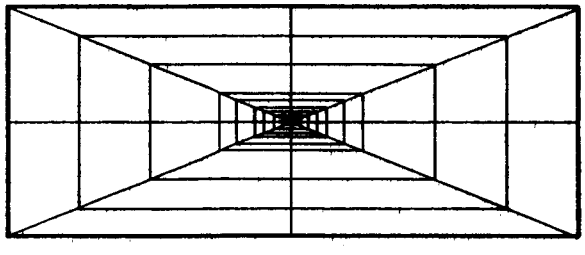

FIGURE 4.- ENLARGED FRONTAL VIEW OF SUPERELEMENT (360 SOLID ELEMENTS: 32-PENTAHEDRONS, 328-HEXAHEDRON; 450 NODES, 1350 DOF).

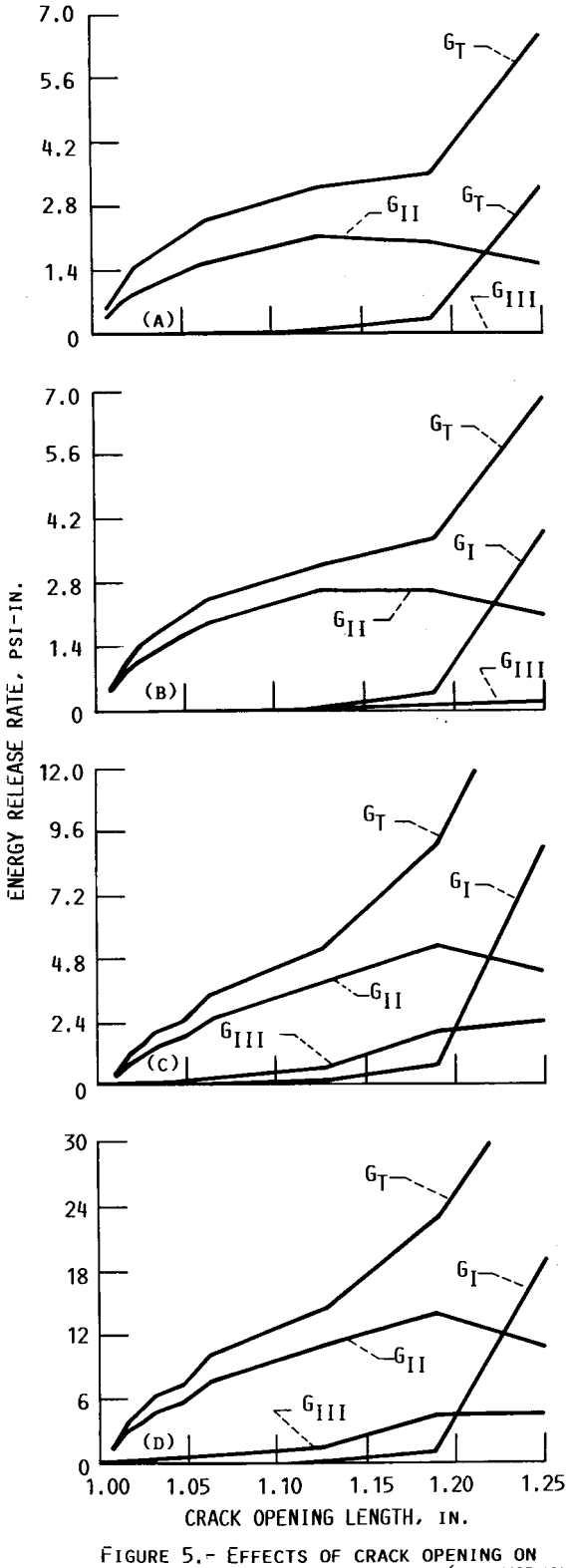

FIGURE 5.- EFFECTS OF CRACK OPENING ON STRAIN ENERGY RELEASE RATES (INDIVIDUAL AND MIXED MODES) FOR DIFFERENT LAMINATE CONFIGURATIONS ($[-\theta_{36}/+\theta_{12}]$; AS-GRAPHITE FIBER/EPOXY (AS-EPOXY), WITH 0.6 FIBER VOLUME RATIO (FVR)) (A) $-\theta = 0^0$; (B) $-\theta = 15^0$; (C) $-\theta = 30^0$; (D) $-\theta = 45^0$; (E) $-\theta = 60^0$; (F) $-\theta = 75^0$; (G) $-\theta = 90^0$.

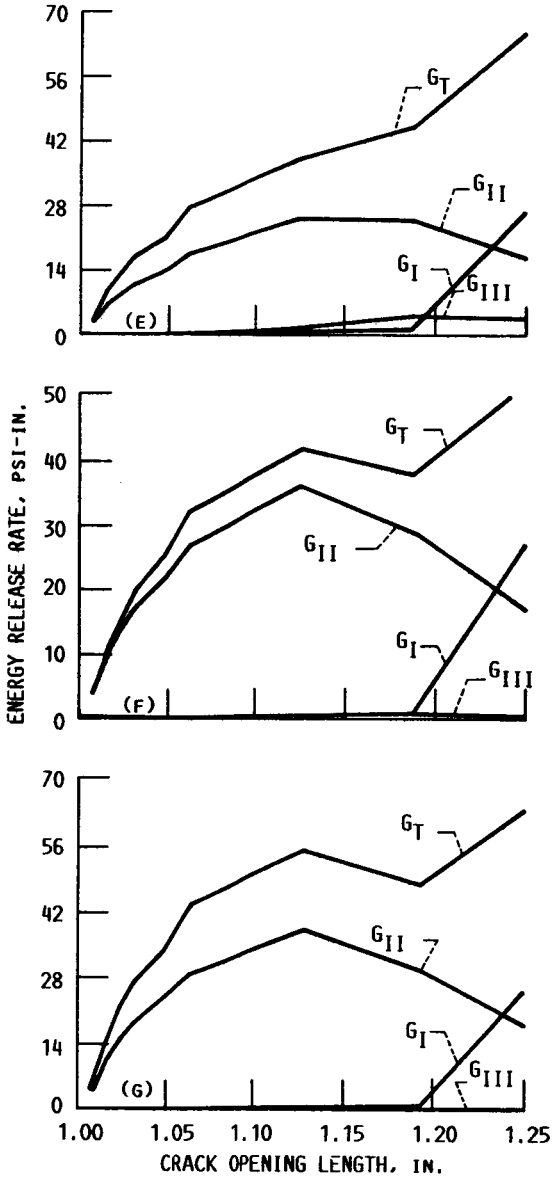

FIGURE 5. - CONCLUDED.

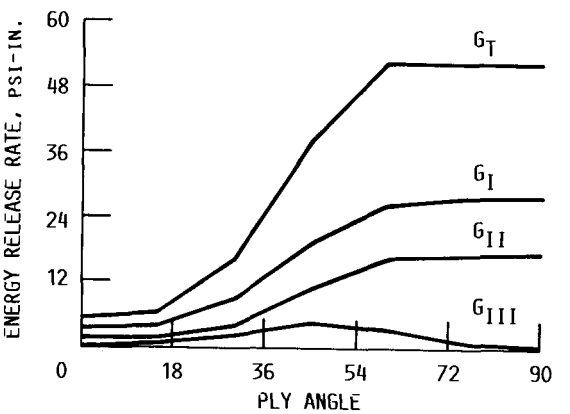

FIGURE 6.- EFFECT OF PLY ORIENTATION ON MAXIMUM INDIVIDUAL AND MIXED MODE STRAIN ENERGY RELEASE RATES ($[-\theta_{36}/+\theta_{12}]$; AS/EPOXY WITH 0.6 FVR).

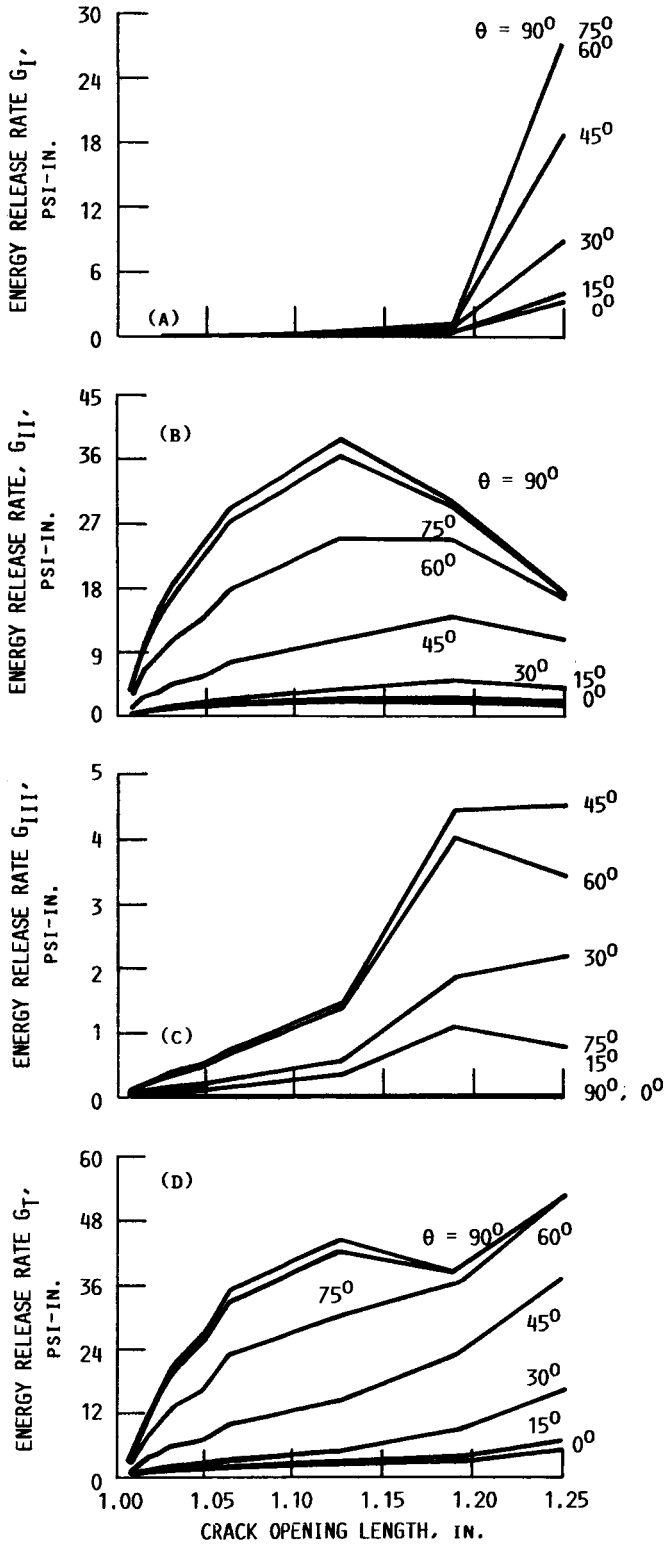

FIGURE 7.- EFFECT OF LAMINATE CONFIGURATION ON STRAIN ENERGY RELEASE RATES ($[-\theta_{36}/+\theta_{12}]$; AS/E WITH 0.6 FVR). A-OPENING MODE (G_I) B-SHEARING MODE (G_{II}), C-TEARING MODE (G_{III}), D-MIXED MODE (G_T).

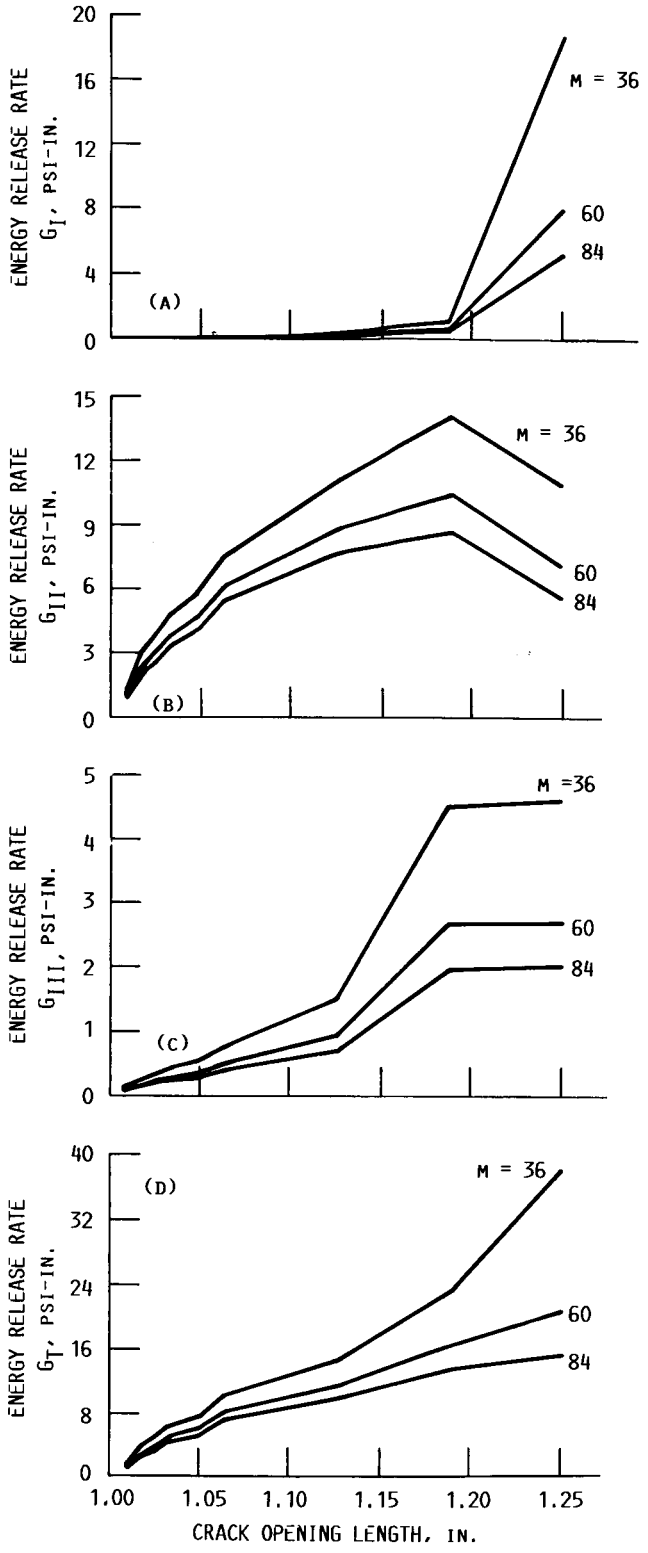

FIGURE 8.- EFFECT OF INTERLAMINAR CRACK LOCATION [$-\theta_M/+\theta_{12}$] ON STRAIN ENERGY RELEASE RATES (AS/E WITH 0.6 FVR). A-OPENING MODE (G_I); B-SHEARING MODE (G_{II}); C-TEARING MODE (G_{III}); D-MIXED MODE (G_T).

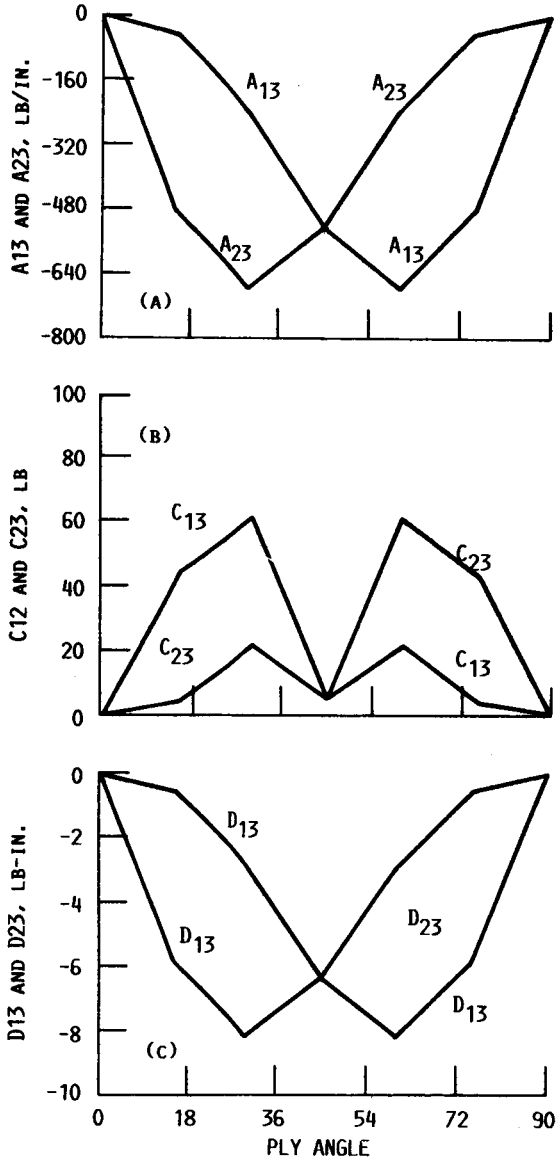

FIGURE 9.- EFFECT OF PLY ORIENTATION ON LAMINATE MATERIAL-COUPLING COEFFICIENT ($[-\theta_{36}/+\theta_{12}]$. AS/E WITH 0.6 FVR).

A-AXIAL NORMAL-SHEAR COUPLING A_{13} AND A_{23};

B-MEMBRANE-BENDING COUPLING C_{13} AND C_{23};

C-BENDING-TWISTING COUPLING D_{13} AND D_{23}.

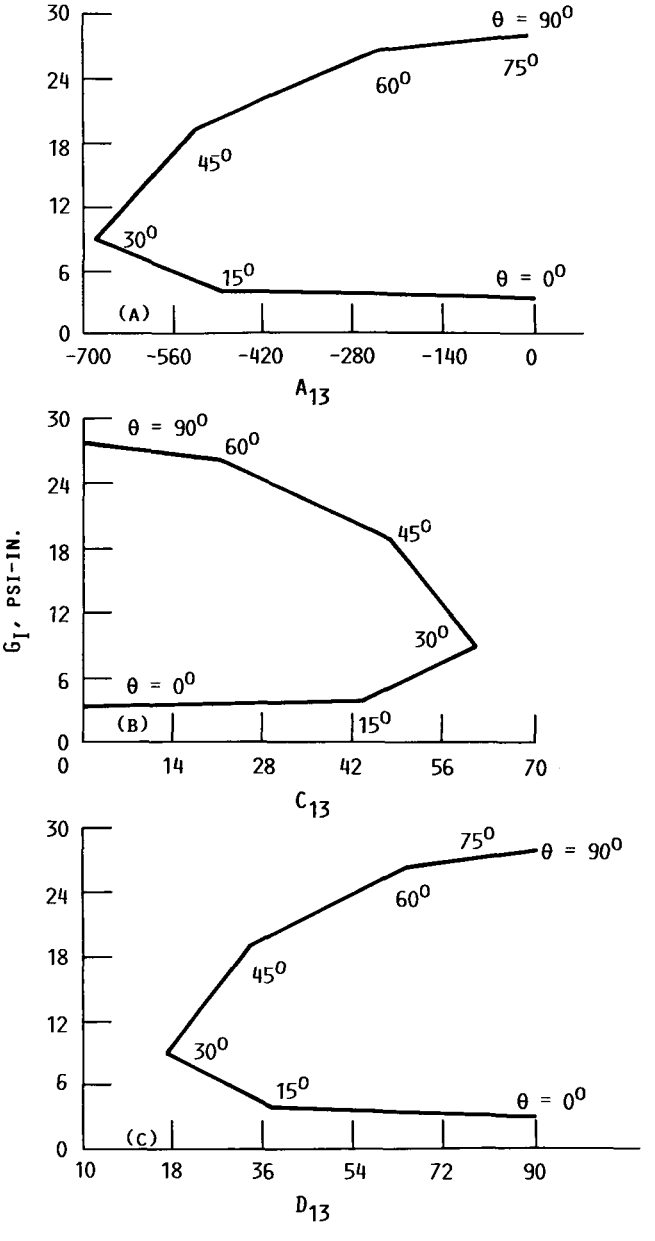

FIGURE 10.- EFFECTS OF LAMINATE MATERIAL-COUPLING COEFFICIENTS ON OPENING MODE STRAIN ENERGY RELEASE RATE (G_I), ($[-_{36}/+_{12}]$, AS/E WITH 0.6 FVR). A-COUPLINE COEFFICIENT A_{13} (LB/IN.); B-COUPLING COEFFICIENT C_{13} (LB), C-COUPLING COEFFICIENT D_{13} (LB-IN.).

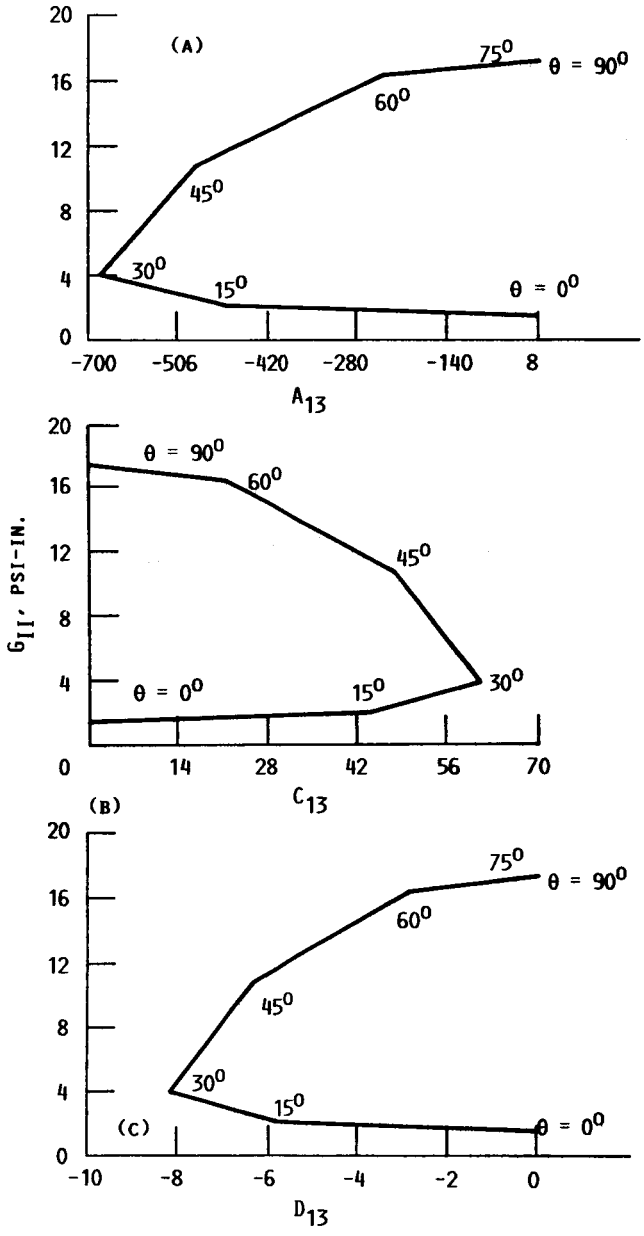

FIGURE 11.- EFFECTS OF LAMINATE MATERIAL-COUPLING COEFFICIENTS ON SHEARING MODE STRAIN ENERGY RELEASE RATE (G_{II}), ($[-\theta_{36}/+\theta_{12}]$, AS/E WITH 0.6 FVR). A-COUPLING COEFFICIENT A_{13} (LB/IN.); B-COUPLINE COEFFICIENT C_{13} (LB); C-COUPLING COEFFICIENT D_{13} (LB-IN.).

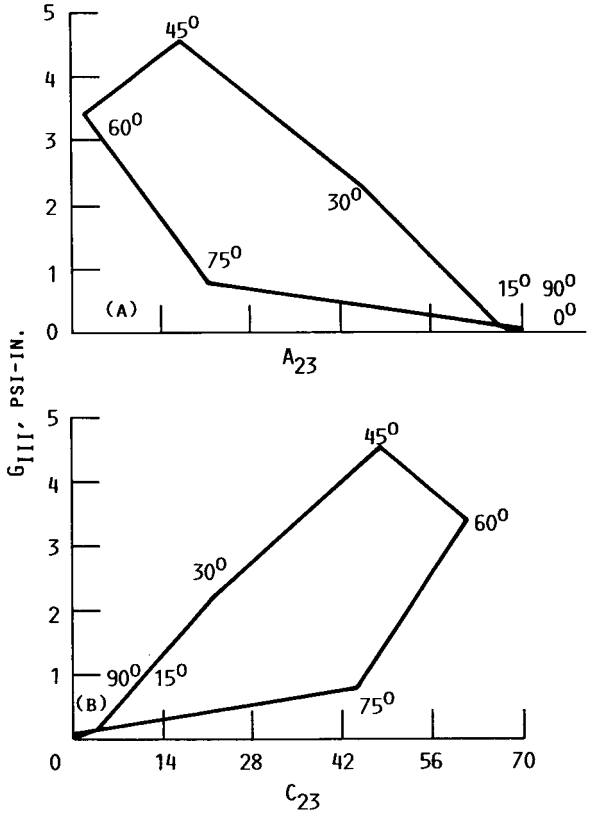

FIGURE 12.- EFFECTS OF LAMINATE MATERIAL-COUPLING COEFFICIENTS ON TEARING MODE STRAIN ENERGY RELEASE RATE (G_{III}), ($[-\theta_{36}/=\theta_{12}]$ AS/E WITH 0.6 FVR).
A.- COUPLING COEFFICIENT A_{23} (LB/IN.);
B.- COUPLING COEFFICIENT C_{23} (LB).

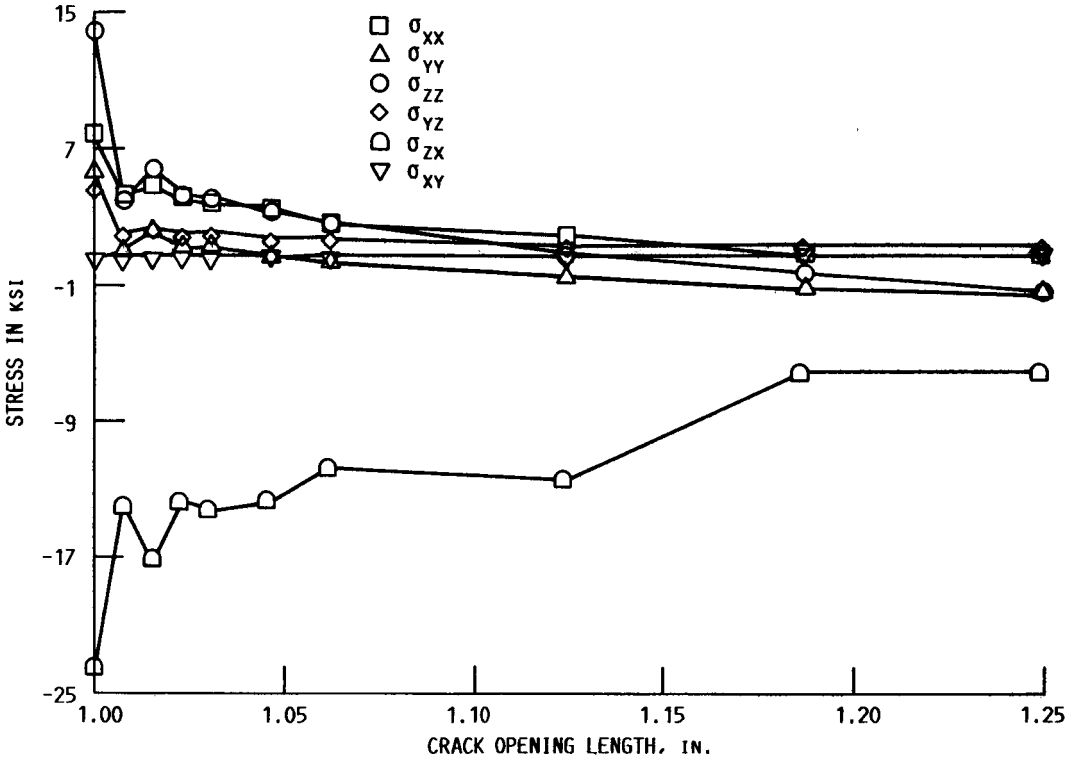

FIGURE 13.- 3-D STRESS STATE IN THE INTERLAMINAR MATRIX LAYER AHEAD OF CRACK TIP ($[-30_{36}/+30_{12}]$. AS/E WITH 0.6 FVR).

1. Report No.	2. Government Accession No.	3. Recipient's Catalog No.
NASA TM-88872		

4. Title and Subtitle	5. Report Date
Composite Interlaminar Fracture Toughness: Three-Dimensional Finite Element Modeling for Mixed Mode I, II, and III Fracture	6. Performing Organization Code: 505-63-11
7. Author(s): Pappu L.N. Murthy and Christos C. Chamis	8. Performing Organization Report No.: E-3278
	10. Work Unit No.
9. Performing Organization Name and Address: National Aeronautics and Space Administration, Lewis Research Center, Cleveland, Ohio 44135	11. Contract or Grant No.
	13. Type of Report and Period Covered: Technical Memorandum
12. Sponsoring Agency Name and Address: National Aeronautics and Space Administration, Washington, D.C. 20546	14. Sponsoring Agency Code

15. Supplementary Notes

Prepared for 8th Symposium on Composite Materials Testing and Design, sponsored by the American Society for Testing and Materials, Charleston, South Carolina, April 28-30, 1986. Pappu L.N. Murthy, Cleveland State University, Cleveland, Ohio 44115 and NASA Lewis Senior Resident Research Associate; Christos C. Chamis, NASA Lewis Research Center.

16. Abstract

A computational method/procedure is described which can be used to simulate individual and mixed mode interlaminar fracture progression in fiber composite laminates. Different combinations of Modes I, II, and III fracture are simulated by varying the crack location through the specimen thickness and by selecting appropriate unsymmetric laminate configurations. The contribution of each fracture mode to strain energy release rate is determined by the local crack closure methods while the mixed mode is determined by global variables. The strain energy release rates are plotted versus extending crack length, where slow crack growth, stable crack growth, and rapid crack growth regions are easily identified. Graphical results are presented to illustrate the effectiveness and versatility of the computational simulation for (1) evaluating mixed-mode interlaminar fracture, (2) for identifying respective dominant parameters, and (3) for selecting possible simple test methods.

17. Key Words (Suggested by Author(s))	18. Distribution Statement
Interlaminar fracture; Fracture modes; Mode I; Mode II; Mode III; Mixed-mode fracture; Fiber composites; Unsymmetric laminates; Strain-energy release-rates; Crack propagation; Material-coupling; Three-dimensional Finite elements; Substructuring; Composite mechanics; Three-dimensional stress analysis; Crack closure; Interply layer	Unclassified - unlimited STAR Category 24

19. Security Classif. (of this report)	20. Security Classif. (of this page)	21. No. of pages	22. Price*
Unclassified	Unclassified		

*For sale by the National Technical Information Service, Springfield, Virginia 22161